s-SNOM imaging of a THz photonic mode

T. Hannotte[1], L. Thomas[1], B. Walter[2], M. Lavancier[1], S. Eliet[1], M. Faucher[1], J.-F. Lampin[1] and R. Peretti[1]

[1]Institut d'Electronique, de Microélectronique et de Nanotechnologie, CNRS, Univ. Lille, Villeneuve d'Ascq, 59652 France

[2]Vmicro SAS, Villeneuve d'Ascq, 59650 France

***Abstract*—We report on the imaging by THz s-SNOM of the field concentration associated to the photonic mode of a split-ring resonator with a 2 µm small gap. The ability to concentrate and probe THz radiations at this scale is of interest for studies on micro and nano objects. Our results are interpreted with numerical calculations as an interplay between the confined near-field and the directional far-field emission of the system.**

I. INTRODUCTION

CONFINEMENT of THz electric fields in small volumes is highly desired to investigate light-matter interactions at sub-λ scales, typically < 100 µm [1]. This is specifically salient for both applied and fundamental purposes. For instance, one can use the field confined in a THz resonator to sense a single nano object placed in a gap of the resonator [2], or to enhance interaction with 2D material to build THz modulators [3] or, on the fundamental side, to enable ultrastrong light-matter interaction at sub-wavelength scale in the THz domain [4]. Such confinement is achieved using THz resonators. Most of them comes from the radar field and can be seen as photonic resonators. These devices are mainly used as a fundamental component of metasurfaces for dispersion properties [5]. In addition to their collective effect on electromagnetic waves, individual resonators often concentrate electric field in gaps as small as a few 10 nm [6] leading to very important field confinement in terms of Purcell's factor when their eigenfrequency is tuned to the incident radiation. As a consequence, an in depth qualitative and quantitative knowledge of both the metasurface and the resonators is an important prerequisite for most of these studies. Since more than 10 years, several groups worldwide put effort in developing THz scattering Scanning Near-field Microscopy (s-SNOM) for this purposes. s-SNOM uses the apex of the tip of an Atomic Force Microscope (AFM) operating in intermittent contact mode as a nano-scatterer used both to couple the THz beam in the resonator and the field of the resonator to the far-field. This technique determines both the radiative and the non-radiative near-field (NF) distribution with a sub-λ resolution while imaging the topography of the sample [7]. However, despite its importance and all the efforts put in, direct characterization of confined THz photonic modes in the NF at such scales remains limited. In this work, we explore the limits of photonic mode near-field imaging by studying the NF distribution of the electric field in split-ring resonators (SRRs) with a THz s-SNOM [8]. We focus on a simple resonator design (see fig 1 A) to confront our results with simulations and physical expectations. We use a probe specifically designed for efficient THz scattering and we propose a physical explanation accounting for the differences between our result and the expected field profile.

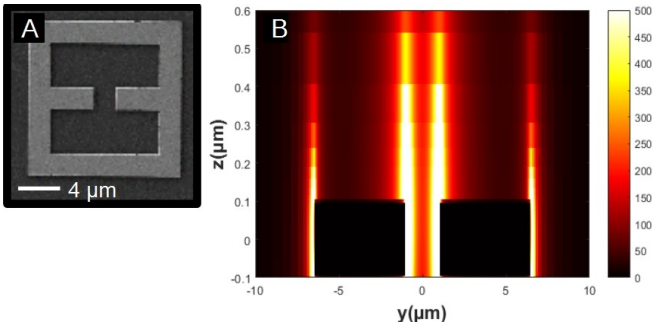

Fig. 1. A: SEM image of one of the fabricated SRRs. This work focuses on the field profile measurement along and above the axis of the central gap. B: Simulated field intensity profile in the YZ plane, with Y being the axis of the gap and Z being the axis perpendicular to the substrate. The SRR is excited with a plane wave. As expected from the Curie's principle, the profile is symmetrical, and the intensity is the same on both sides of the gap.

II. KEY ELEMENTS DESIGN

The main elements of a s-SNOM experiment are the sample, the probe, and the optical setup for illumination and detection. We use a standard optical setup and the neaSNOM platform similar to the ones presented in [7]. Here we focus on the design and fabrication of the most significant elements for our problematic: the resonator and the scanning probe. The chosen geometry for our resonator is a double loop SRR (fig. 1 A). It is one of the simplest geometry, with the electric field confined in a single area at the resonance, and a good quality factor compared to the single loop SRR since the magnetic radiation cancels in the far-field. We use high resistivity silicon substrate (>10 000 Ωcm) for its low absorption and low dispersion in the THz range [9,10]. Electromagnetic simulation with the FDTD software from Lumerical predict the confinement of the electric field in the gap and its extension to the branches of the capacitive element atop the device (fig. 1 B). We fabricated the SRRs starting with a 300 µm high resistivity silicon wafer using an electron beam lithography process and electron beam metal evaporation as described in [11]. Figure 1 A shows a SEM picture of one of the fabricated SRRs. We fabricated several array of SRRs with slightly different size (from 13 µm to 17 µm) in order to tune the resonance frequency. We measured their transmission spectrum with time domain terahertz spectroscopy. The transmission spectrum of an array of resonators shows a minimum in transmission at the resonance frequency [6]. Based on those spectra, we chose the best SRR dimensions for a resonance at 2.5 THz, frequency of the CO_2 pumped methanol gas laser, which is our excitation source for s-SNOM experiments. Those dimensions are 13 µm size, 200 nm thick, and 2 µm gap. The s-SNOM tip used for all the experiment was a Lprobe model 'CT' from Vmicro [12]. This probe is especially designed for THz s-SNOM experiment. In

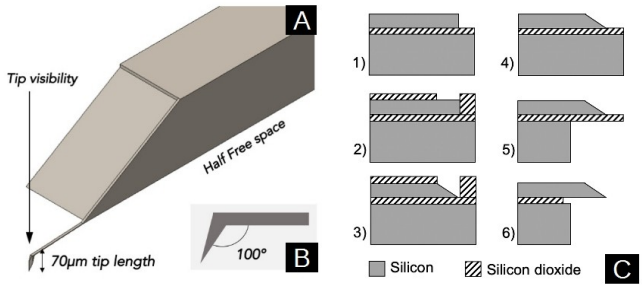

Fig. 2. A: Schematic view of the Lprobe cantilever and its holder. The cantilever and the tip are placed at one corner of the holder. The free solid angle around the tip is extended compared to commercial probes thanks to the half free space given by the specific shape of the cantilever holder. B: The angle between the tip and the cantilever let an optical path to see the tip end from the top. C: Process flow for Lprobe micro-fabrication. 1) Initial patterning 2) Hard mask deposition 3) Chemical etching 4) Hard mask removal 5) Back side plasma etching 6) HF etching.

fact, Maissen *et al.* demonstrated that the imaging resolution can be greatly increased by using long and ultrasharp s-SNOM tips, and achieved resolution down to 15 nm [13]. Additionally, s-SNOM tip can be modeled as a dipole antenna excited by the near field concentration on the sample; hence, a longer tip (close to the excitation wavelength) will have a better scattering efficiency despite the small apex. The Lprobe aims at coping with these issues. The fabrication process of such probes differs from all other commercially available cantilevers. The Lprobes are fabricated on a SOI (Silicon On Insulator) wafer. The cantilever and the tip are fabricated in the wafer plane, in the Device Layer (Dl) which is the top silicon layer of the SOI wafer. At the end of the process, the chip is rotated 90° around the cantilever axis inside the AFM head so the tip is pointing down. The fabrication process gives access to a wide range of cantilever parameters regarding the resonant frequencies and stiffnesses as well as tip geometry. The angle between the tip and the cantilever can be tuned between + and - 45° around the orthogonal position (90°). In this work, the angle between the tip and the cantilever is 100° (fig. 2 B) and the tip length is 70µm. This configuration enables the tip visualization from above and eases the s-SNOM experiment as illustrated in figure 2 A. The cantilever stiffness is 40 N/m and the resonant frequency of the fundamental mode measured in the complete neaSNOM setup is 280 kHz. In figure 2 C, we present the simplified process flow implemented by Vmicro : i) The starting material is a SOI wafer. A first photolithography step defines the cantilever and the chip area. Then a vertical plasma etching step is used to transfer the resist pattern into the silicon device layer. ii) An oxide hard mask is deposited on top of the silicon wafer and patterned using a second photolithography step and another plasma etching. iii) Anisotropic chemical etching of the silicon is performed using a KOH solution. The chemical etching stops on the <111> plane. iv) The oxide hard mask is removed using an HF acid solution. v) Back side plasma etching defines the AFM chip. vi) A final hydrofluoric chemical etching removes the buried oxide of the SOI wafer.

On figure 3 B, we present the fabricated cantilever with up to 70 µm long tips. Since the cantilevers and the tips are batch-fabricated, geometrical parameters and mechanical parameters

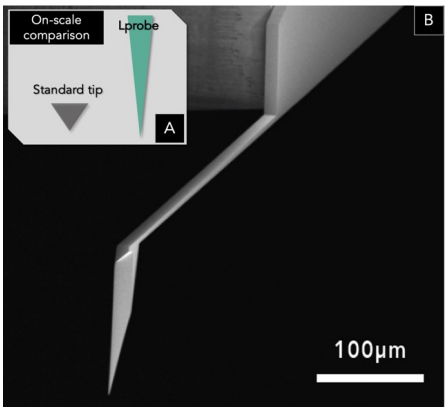

Fig. 3. A: on-scale comparison of tip aspect ratio between a standard tip (pyramidal shape) and the Lprobe tip. B: SEM image of the Lprobe cantilever and tip.

are reproducible with dispersion less than 5%. Getting back to the probe properties described by Maissen *et al.* for nanoscopic resolution [13], the schematic on figure 3 A is an on-scale comparison of a standard tip i.e. a pyramidal shape with a total angle of 35° at the tip apex. The Lprobe tip apex angle is below 15°. The consequence is an aspect ratio improved by a factor 2. s-SNOM experiments were carried out on the SRRs fabricated by e-beam lithography. Our setup operates in a homodyne detection scheme and optical signals are demodulated at the 2nd harmonic of the oscillation of the probe.

III. Results

The THz s-SNOM images (fig. 4) exhibited two distinct features: a bright region from the gap to the left branch of the capacitor corresponding to the photonic mode and an extinction of the optical signal on the right of the resonator. The topography showed no difference between these two regions. Here we notice two major difference between the simulated field profile and the s-SNOM measurement : a weaker intensity inside the gap and a strong asymmetry between each side of the gap. The first point is explained by the vertical geometry of the probe. Such a probe will act as a dipole antenna when polarized in its longer dimension; we therefore expect a much more efficient scattering of the near-field when the last is oriented along the Z axis. To better depict this effect, figure 5 shows the field intensity profile projected on the Z axis. The projected field is indeed much weaker inside the gap than on top of the branches close to it, which is coherent with the left side of the s-SNOM picture. Yet it does not account for the dark region measured on the entire right side. To explain the asymmetry of the result, one have to consider the asymmetry of the whole measurement setup (see reference [7] for multiple setup examples). In most s-SNOM apparatus including ours, the most significant asymmetry comes from the parabolic mirror used to focus the excitation light on the sample and to collect the light scattered from the probe [7]. This mirror only collect the scattering light over a limited solid angle, hence the detected signal is a good indication of the near-field intensity only if we consider the scattering far-field pattern to be independent from the probe position on the sample. However, although both the probe and

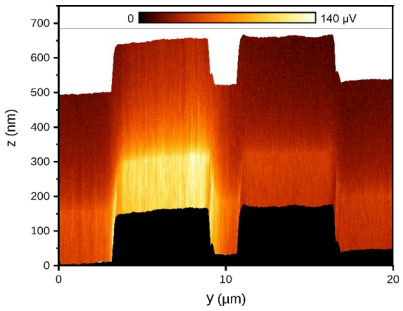

Fig. 4. Measured s-SNOM signal in the Y Z plane. The black area is the sample topography. The detected signal is strong above the left branch with a maximum close to the gap, while almost no contrast compared to the substrate is observed on the right branch.

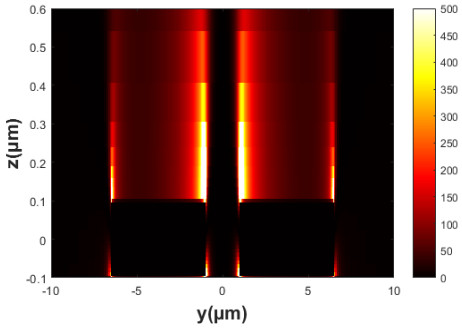

Fig. 5. Intensity profile of the simulated electric field projected on the Z axis, on the same plane as in Fig. 1 B. The intensity of the projected field is close to zero inside the gap as the field is mainly perpendicular to the metal surface.

the SRR are expected to have a symmetrical scattering radiation pattern when taken independently, the combination forms a complex antenna whose emission pattern cannot be assumed independent from the probe position [14]. More concretely, we expect a strong signal when the far-field emission pattern of the probe-sample antenna is directed toward the parabolic mirror and a weak signal when it is not. From the point of view of figure 4, the parabolic mirror in our experiment is placed on the right side of the picture, thus our data implies that when the s-SNOM probe is located above one branch of the SRR, the scattered field is preferably directed toward the opposite branch of the SRR.

Considering the yet unknown dependency of the far-field emission pattern on the probe position, deducing a quantitative map of the SRR near-field profile from s-SNOM data will require further far-field characterization of the apparatus.

IV. Summary

To sum up, we conducted an experiment where we imaged by THz s-SNOM the field confinement associated to the photonic mode of a SRR. The experiment was realized with control over the SRR fabrication, the probe fabrication and the s-SNOM setup. Numerical simulations were used to test the viability of our measurements. The interpretation of the obtained images is non-trivial and strongly deviates from the intuitive assumptions that the detected signal directly scales with the near-field intensity at the probe apex. The directivity of the scattering clearly has a very significant effect on the measured signal, and the near-field profile of a metallic structure such as a SRR cannot be directly deduced from the s-SNOM image without a precise understanding of the far-field emission pattern of the system. We are now investigating new routes for THz s-SNOM to image the full NF distribution and aim to reduce gap size to achieve even narrower confinement.

V. Acknowledgments

This work was supported by the international chair of excellence "ThOTroV" from region "Hauts-de-France", the National Research Agency (ANR) under program ExCELSiOR ANR 11-EQPX-0015, the welcome talent grant NeFiStoV from European metropole of Lille, the French RENATECH network on micro and nanotechnologies and the LabCom Horiba IEMN.

References

[1]. G. R. Keiser and P. Klarskov, "Terahertz Field Confinement in Nonlinear Metamaterials and Near-Field Imaging," Photonics, vol. 6, pp. 1-27, Feb., 2019.

[2]. S. J. Park, J. T. Hong, S. J. Choi, H. S. Kim, W. K. Park, S. T. Han, J. Y. Park, S. Lee, D. S. Kim and Y. H. Ahn, "Detection of microorganisms using terahertz metamaterials", Scientific Reports, Springer Science and Business Media LLC, 2014, 4.

[3]. R. Degl'Innocenti, D. S. Jessop, Y. D. Shah, J. Sibik, J. A. Zeitler, P. R. Kidambi, S. Hofmann, H. E. Beere and D. A. Ritchie, "Low-Bias Terahertz Amplitude Modulator Based on Split-Ring Resonators and Graphene", ACS Nano, American Chemical Society (ACS), 2014, 8, 2548-2554.

[4]. C. Maissen, G. Scalari, F. Valmorra, M. Beck, J. Faist, C. Cibella, R. Leoni, C. Reichl, C. Charpentier and W. Wegscheider, "Ultrastrong coupling in the near field of complementary split-ring resonators", Physical Review B, American Physical Society (APS), 2014, 90.

[5]. S. Liu, A. Noor, L. L. Du, L. Zhang, Q. Xu, K. Luan, T. Q. Wang, Z. Tian, W. X. Tang, J. G. Han, W. L. Zhang, X. Y. Zhou, Q. Cheng and T. J. Cui, "Anomalous Refraction and Nondiffractive Bessel-Beam Generation of Terahertz Waves through Transmission-Type Coding Metasurfaces", ACS Photonics, American Chemical Society (ACS), 2016, 3, 1968-1977.

[6]. T. Hannotte, M. Lavancier, S. Mitryukovskiy, J.-F. Lampin and R. Peretti, "Terahertz radiation confinement using metallic resonators", 2019 44th International Conference on Infrared, Millimeter, and Terahertz Waves (IRMMW-THz), IEEE, 2019.

[7]. X. Chen, D. Hu, R. Mescall, G. You, D. N. Basov, Q. Dai and M. Liu, "Modern Scattering-Type Scanning Near-Field Optical Microscopy for Advanced Material Research," Advanced Materials, 1804774, 2019.

[8]. A. J. Huber, F. Keilmann, J. Wittborn, J. Aizpurua and R. Hillenbrand , "Terahertz Near-Field Nanoscopy of Mobile Carriers in Single Semiconductor Nanodevices," NANO LETTERS, vol. 8, pp. 3766-3770, 2008.

[9]. R. Peretti, S. Mitryukovskiy, K. Froberger, M.A. Mebarki, S. Eliet, M. Vanwolleghem and J.-F. Lampin, "THz-TDS Time-Trace Analysis for the Extraction of Material and Metamaterial Parameters" IEEE Transactions on Terahertz Science and Technology, Institute of Electrical and Electronics Engineers (IEEE), 2019, 9, 136-149.

[10]. J. Dai, J. Zhang, W. Zhang and D. Grischkowsky, "Terahertz time-domain spectroscopy characterization of the far-infrared absorption and index of refraction of high-resistivity, float-zone silicon", Journal of the Optical Society of America B, The Optical Society, 2004, 21, 1379

[11]. T. Hannotte, L. Thomas, M. Lavancier, S. Mitryukovskiy, J.-F. Lampin and R. Peretti, "Towards broadband THz spectroscopy and analysis of subwavelength size biological samples in Terahertz Photonics" SPIE, 2020.

[12]. B. Walter, E. Mairiaux, D. Vignaud, S. Eliet, J.-F. Lampin and M. Faucher, "Terahertz near-field imaging using batch-fabricated cantilevers with 70 µm long tips," *44th IRMMW-Thz conference*, pp. 1-2, Paris, France, 2019.

[13]. C. Maissen, S. Chen, E. Nikulina, A. Govyadinov and R. Hillenbrand, "Probes for Ultrasensitive THz Nanoscopy," ACS Photonics, American Chemical Society (ACS), 2019, 6, 1279-1288.

[14]. R. Lecaque, S. Grésillon, N. Barbey, R. Peretti, J.-C. Rivoal and C. Boccara, "THz near-field optical imaging by a local source", Optics Communications, Elsevier BV, 2006, 262, 125-128.